Anal. Chem. **2009,** *81,* 6805–6812

Threshold Collision-Induced Dissociation Measurements Using a Ring Ion Guide as the Collision Cell in a Triple-Quadrupole Mass Spectrometer

Vladimir Romanov, Udo H. Verkerk, Chi-Kit Siu, Alan C. Hopkinson, and K. W. Michael Siu*

Department of Chemistry and Centre for Research in Mass Spectrometry, York University, Toronto, Ontario, Canada M3J 1P3

A triple-quadrupole mass spectrometer has been modified for bond-dissociation energy measurements via threshold collision-induced dissociations (TCIDs) by replacing the conventional collision cell with a ring ion guide. Optimal operating conditions for the ring ion guide were determined or derived, and validated using a set of complexes for which bond dissociation energies are known. A comparison with reference data (within a range of 16−57 kcal/mol) indicates an accuracy approaching that of TCID determined on a guided ion-beam mass spectrometer. Complexes for which bond-dissociation energies were measured include metal ion complexes of simple ligands, amino acids and peptides, as well as of carbonic acid. There is excellent agreement between our experimental data and literature data, as well as theoretical data determined using a high-level computational method.

Noncovalent interactions play the key role in maintaining secondary and tertiary structures that determine the form and function of enzymes and other proteins.[1] As a result of the development of electrospray ionization,[2] biologically relevant model systems can now be examined in the absence of solvent interactions, thereby allowing a comparison of intrinsic binding as determined experimentally with that calculated from first-principle methods. Such quantitative analyses of bond strengths shed light on noncovalent interactions in larger biological systems. Because of the cumulative nature of weak interactions in large systems, highly accurate bond-dissociation data are required and new instrumentation continues to be developed for such purposes. Historically, bond energies have been determined using various mass spectrometric techniques, including the equilibrium,[3] bracketing,[4] and kinetic[5] methods, as well as threshold collision-induced dissociation (TCID),[6] blackbody infrared radiative dissociation (BIRD),[7] and surface-induced dissociation (SID).[8] The majority of the instrumentation used is Fourier-transform ion cyclotron resonance-based or specifically built for the sole purpose of obtaining thermodynamic data. Of the aforementioned methods, TCID allows investigation of the widest range of bond energies, and is increasingly being applied to molecules that are important in organometallic chemistry, catalysis, and supramolecular chemistry.[9,22] As a result of the pioneering studies of Armentrout and co-workers,[10] TCID is now an established method for obtaining accurate bond-dissociation energies.

Toward that end, the TCID method requires that the onset of the precursor ion fragmentation be modeled via curve-fitting of the product channel's cross section as a function of the center-of-mass collision energy. This onset then gives the bond-dissociation energy (Table 1). In practice, for larger precursor ions, additional internal energy is required to ensure that fragmentation occurs inside the collision cell, and a correction is applied to the apparent threshold for this kinetic shift, whose magnitude can be estimated from the unimolecular rate constant of the dissociation according to the Rice−Ramsperger−Kassel−Marcus (RRKM) theory.[11]

To ensure well-defined energy transfers, single-collision conditions are required, which is ascertained by extrapolating the cross sections measured under low-pressure conditions to zero collision-gas pressure.[12] The collection efficiency of the collision cell must be high because of the low abundance of product ions; under typical low-pressure conditions, the reaction efficiency is less than 20%.[13] The dissociation, extraction, and detection of ions should be free from mass discrimination. In addition, the precursor ion should yield an ensemble of product ions that have well-defined internal (E_i) and kinetic energies (E). These requirements have been discussed in a number of reviews and articles by

* To whom correspondence should be addressed. Professor K. W. Michael Siu, Department of Chemistry and Centre for Research in Mass Spectrometry, York University, 4700 Keele Street, Toronto, Ontario, Canada M3J 1P3. Phone: (416)-650-8021. Fax: (416)-736-5936. E-mail: kwmsiu@yorku.ca.

(1) Desiraju, G. R. *Nature* **2001**, *412*, 397–400.
(2) Yamashita, M.; Fenn, J. B. *J. Phys. Chem.* **1984**, *88*, 4451–4459.
(3) Kebarle, P. *J. Am. Soc. Mass Spectrom.* **1992**, *3*, 1–9.
(4) Gorman, G. S.; Amster, I. J. *J. Am. Chem. Soc.* **1993**, *115*, 5729–5735.
(5) Cooks, R. G.; Koskinen, J. T.; Thomas, P. D. *J. Mass Spectrom.* **1999**, *34*, 85–92.
(6) Rodgers, M. T.; Armentrout, P. B. *Mass Spectrom. Rev.* **2000**, *19*, 215–247.
(7) Dunbar, R. C. *Mass Spectrom. Rev.* **2004**, *23*, 127–158.
(8) Laskin, J. *Eur. J. Mass Spectrom.* **2004**, *10*, 259–267.
(9) Rodgers, M. T.; Armentrout, P. B. *Acc. Chem. Res.* **2004**, *37*, 989–998.
(10) Ervin, K. M.; Armentrout, P. B. *J. Chem. Phys.* **1985**, *83*, 166–189.
(11) Rodgers, M. T.; Ervin, K. M.; Armentrout, P. B. *J. Chem. Phys.* **1997**, *106*, 4499–4508.
(12) Schultz, R. H.; Crellin, K. C.; Armentrout, P. B. *J. Am. Chem. Soc.* **1991**, *113*, 8590–8601.
(13) Romanov, V.; Siu, C.-K.; Verkerk, U. H.; El Aribi, H.; Hopkinson, A. C.; Siu, K. W. M. *J. Phys. Chem. A.* **2008**, *112*, 100912–100920.

10.1021/ac9009758 CCC: $40.75
Published on Web 07/27/2009

Table 1. Equations Used for Deriving Bond Energies from TCID Measurements[a]

$$\sigma_p(E_{CM}) = \sigma_0 \sum_i g_i(E_{CM} + E_i + E_0)^n/E_{CM} \quad (1)$$

$$\sigma_p = \frac{I_{prod}}{(I_{reac} + I_{prod})nl} \quad \text{where } nl\sigma_p \ll 1, \text{ see ref 16} \quad (2)$$

$$E_{CM} = E_{lab}m_{Ar}/(m_{parent} + m_{Ar}) \quad (3)$$

[a] σ_p (E_{CM}), collision cross section as a function of parent ion kinetic energy; σ_0, scaling factor; E_{cm}, energy of parent ion in center-of-mass frame of reference; E_0, threshold (bond dissociation) energy to be determined; E_i, internal energy of a given vibrational state with a relative population g_i; n, adjustable parameter. σ_p, Collision cross section of product ion p at a specific kinetic energy; I_{prod}, ion intensity of daughter ion; I_{reac}, ion intensity of parent ion; n, collision gas density; l, collision cell length. E_{lab}, energy of parent ion in laboratory frame of reference; m_{Ar}, mass of collision gas; m_{parent}, mass of parent ion.

Armentrout and co-workers.[10,14−16] The traditional guided ion-beam mass spectrometer (GIBMS) used in TCID experiments comprises an ion source, mass selector and ion guide with a collision cell, mass analyzer, and detector. In this setup, the complete collection of scattered primary and secondary ions is ensured through the use of a cylindrical effective potential generated by the rf field of the ion guide.[17] An essential element of thermodynamic measurements performed on such a setup is the careful selection of ion optical elements and potentials applied to these elements to achieve minimal perturbation of the initial, well-characterized internal and kinetic energy distribution of the precursor ions and near-ideal conditions for collecting the product ions after collision-induced dissociation.

A conventional triple-quadrupole mass spectrometer might appear, at first glance, a suitable instrument for conducting TCID experiments. In practice, the collision cell (q2) of a triple-quadrupole mass spectrometer may result in scattering of ions out of the phase space acceptance of the downstream resolving quadrupole.[18] Because the fragment ions generated in TCID have lower mass and energy than the precursor ions, differences in the ion transmission may result in unintended mass discrimination. In addition, in most quadrupole mass spectrometers, the rf voltage of the collision cell follows the driving rf of one of the resolving quadrupoles through a capacitive divider.[18] Although no resolving dc component is present in q2, the rf amplitude is reduced, thus emphasizing differences in the containment of ions with different mass. Fringe fields between quadrupole rod sets contribute further uncertainty with regard to mass discrimination and internal energy of the ions. In short, while the triple-quadrupole mass spectrometer offers many analytical advantages,[17,19] ions are exposed to various degrees of rf heating, thus resulting in an ill-defined distribution of internal energies.[20] Radio frequency heating of ions is the result of an increase in kinetic and internal energy (through collisions with neutral gas) when ions approach the quadrupole rods due to an insufficiently steep effective potential. Nevertheless, TCID measurements have been implemented on *modified* triple-quadrupole instruments.[21,22] In general, these measurements require the assumption of complete thermalization of the precursor ions before collision with a stationary inert gas (vide infra). As a result, the quality of the data obtained on a triple-quadrupole mass spectrometer is considered inferior to that obtained on the GIBMS.[10,14−16]

To minimize any increase in ion internal energy, the average time that the ions interact with the rf field must be minimized, while still maintaining ion confinement.[17] This can be achieved by increasing the number of rods in the collision cell beyond four, resulting in the creation of a larger field-free region between the rods and a steeper field near the rods relative to the quadrupole. Such higher-order multipoles are additionally characterized by an efficient 4π steradian collection of scattered ions;[17,23] however, the characteristic mass-selecting capability of the quadrupole is lost in hexapoles and octopoles. To achieve both ion selection and ion confinement, the tandem of a quadrupole and multipole is, therefore, used.[10,17] A parallel development sees the application of adiabatic approximation for inhomogeneous rf fields by Teloy and Gerlich,[17,19,23] which led to development of the axially symmetric ring ion guide. Ring ion guides have been used as ion funnels for efficient ion sampling and transport[24] in low-temperature trapping experiments[25] and recently in ion-mobility experiments.[26] The ring ion guide should be suitable for use as a collision cell in TCID experiments, based on its excellent ion-containing properties which are comparable to 22-pole ion guides.[19,37] Although multipole ion guides have been used in TCID experiments,[22] ring ion guides offer greater ease of construction and flexibility in gas-phase ion chemistry (vide supra). Here we describe the adaptation and validation of a modified triple-quadrupole mass spectrometer for use in TCID experiments after having the spectrometer's q2 collision cell replaced with a ring ion guide.

EXPERIMENTAL SECTION

Chemicals. All chemicals were obtained from Sigma-Aldrich, St. Louis, MO, and were used without further purification. Sample solutions were 100 μM in ferriprotoporphyrin IX chloride (hemin), amino acids (glycine and proline) and tripeptides (triglycine, GGG,

(14) Armentrout, P. B. *J. Am. Soc. Mass Spectrom.* **2002**, *13*, 419–434.
(15) Armentrout, P. B. *Top. Curr. Chem.* **2003**, *225*, 233–262.
(16) Armentrout, P. B. *J. Anal. At. Spectrom.* **2004**, *19*, 571–580.
(17) Gerlich, D. RF Ion Guides In *The Encyclopedia of Mass Spectrometry*; Gross, M. L., Caprioli, R., Eds.; Elsevier: Amsterdam, The Netherlands, 2003, Vol. 1, pp 182−195.
(18) Thomson, B. A.; Douglas, D. J.; Corr, J. J.; Hager, J. W.; Jolliffe, C. L. *Anal. Chem.* **1995**, *67*, 1696–1704.
(19) Gerlich, D. *Adv. Chem. Phys.* **1992**, *82*, 1–176.
(20) Ryjkov, V. L.; Zhao, X.; Schuessler, H. A. *Phys. Rev. A* **2005**, *71* (033414), 1–4.
(21) Klassen, J. S.; Kebarle, P. *J. Am. Chem. Soc.* **1997**, *119*, 6552–6563.
(22) Zocher, E.; Dietiker, R.; Chen, P. *J. Am. Chem. Soc.* **2007**, *129*, 2476–2481.
(23) Gerlich, D. *J. Anal. At. Spectrom.* **2004**, *19*, 581–590.
(24) Ibrahim, Y.; Tang, K.; Tolmachev, A. V.; Shvartsburg, A. A.; Smith, R. D. *J. Am. Soc. Mass Spectrom.* **2006**, *17*, 1299–1305.
(25) Savic, I.; Cermak, I.; Gerlich, D. *Int. J. Mass Spectrom.* **2005**, *240*, 139–147.
(26) Giles, K.; Pringle, S. D.; Worthington, K. R.; Little, D.; Wildgoose, J. L.; Bateman, R. H. *Rapid Commun. Mass Spectrom.* **2004**, *18*, 2401–2414.

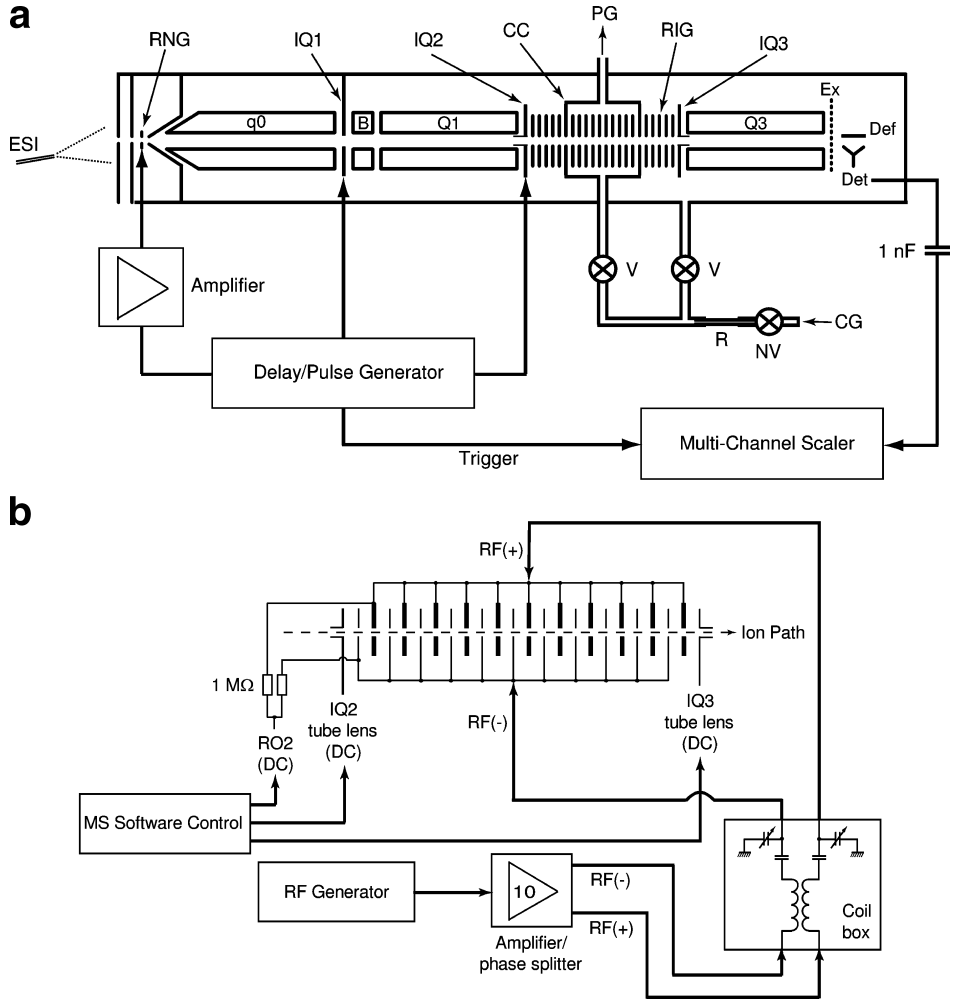

Figure 1. (a) Schematic of the API 365 triple quadrupole mass spectrometer after replacement of the q2 collision cell with a ring ion guide collision cell. CC, collision cell; CG, collision gas; V, valve; NV, needle valve; R, restrictor; RIG, ring ion guide; PG, pressure gauge; B, Brubaker lens; IQ1,2,3, interquad lenses; Def, deflector; Det, detector; Ex, extraction lens. Also shown is the pulse generator connected through an amplifier to the ring electrode (RNG) for measuring the overall travel time through the mass spectrometer. By connection of IQ1 to the pulse generator, the time spent outside q0 by an ion pulse can be measured. For determination of the zero of the energy scale and the kinetic energy distribution, IQ2 is connected to the pulse generator. In all cases, a multichannel scaler is used for recording. During such measurements, ion optical elements that are being pulsed externally are disconnected from the API 365 electronics. (b) Schematic of the electrical connections between the ring ion guide, the rf generator, amplifier, coil box, and the existing DAC lines of the API 365.

and trialanine, AAA), and 50 μM in metal salts (silver nitrate, sodium as well as potassium nitrate and bicarbonate) in 20/80 water/methanol. The sample solution was infused into the pneumatically assisted electrospray source (vide infra) at a typical flow rate of 3 μL/min and at a potential of 5 kV, with nitrogen being the nebulizer and curtain gas.

Instrumentation. *Mass Spectrometer.* All experiments were performed on a modified API 365 triple-quadrupole mass spectrometer (Applied Biosystems/MDS SCIEX, Concord, ON). The quadrupole collision cell was disconnected from the rf leads to Q3 and replaced by a ring ion guide that is reversibly mounted on the ion optics rail of the API 365 and driven by an independent rf source (see Figure 1 and the Supporting Information for additional details). The Interquad 2 and 3 lens voltages (IQ2, IQ3), together with the offset voltage (RO2), were coupled to the ring ion guide (see Figure 1b) and controlled using the manufacturer's LC2Tune software (version 1.4). TCID measurements were automated using the MRM option in this software, using a dwell time of 10 s/voltage step (for the pulsed beam experiment, 20 s/voltage step) for each channel observed. The step size was varied between 0.1 and 0.5 V so that 100 data points over the entire kinetic energy range were obtained. Collision gas was introduced into the ring ion guide via a stainless steel capillary (0.005 in. i.d., Supelco, Bellefonte, PA) and adjusted by a needle valve (Swagelok, Solon, OH) connected to a 1 L argon gas reservoir at a pressure of 2−30 psi. Pressure in the ring ion guide was measured using a Baratron absolute pressure transducer (type 627B, MKS Instruments, Wilmington, MA) together with a readout unit (type 660, MKS Instruments).

Ring Ion Guide. A ring ion guide of 210 mm in length was constructed from 194 triangular gold-plated copper plates—each 0.4 mm thick with an axial aperture of 5 mm in diameter—mounted on a gold-plated, double-sided, printed circuit board (PCB). Alignment of the plates was attained using two alumina guides with 194 slots machined on each side to maintain an interplate distance of 0.6 mm along the whole axis. Within the ring ion guide, a collision cell with a length of 130 mm was formed by the alumina guides and a gold-plated, double-sided PCB top cover on which a

$^1/_4$ in. adapter (Swagelok) for a fluorinated corrugated tube (Cole-Parmer Inc., Vernon Hills, IL) was mounted for connection to the pressure transducer. Positioning of the collision cell in the middle of the ring ion guide ensured minimal influence of the fields generated by Q1 and Q3 and separated the region of rapid kinetic energy change from that of high gas number density (vide infra). The argon collision gas was contained by closing the box with two square (instead of triangular) gold-plated copper plates, each with an aperture of 5 mm in diameter. Argon was introduced through a hole in the mounting PCB. The first and last plates of the ring ion guide had each a 8 mm long press-fitted tube mounted as a tube lens.[27] The first and last 40 mm of each alumina guide contained three holes (diameter, 8 mm), thereby ensuring a well-defined axial gas density distribution within the ring ion guide. The ring ion guide was mounted between Q1 and Q3, such that the two tube lenses protruded approximately 2 mm into the Q1 and Q3 rod sets.

The time-of-flight distribution was registered for short ion pulses using a fast multichannel scaler (Stanford Research Systems, model SR 430, resolution 320 ns) by accumulating 60 000 scans. Ion pulse sequences and the start/stop signal for the multichannel scaler were programmed in a four-channel digital delay/pulse generator (Stanford Research Systems, model DG 535) with an adjustable offset and amplitude between −3 and +4 V dc with a 4 V maximum step-size. For pulsing of the ring electrode, higher voltages were required to prevent ions from entering q0; this was implemented using a fast custom-built amplifier with variable output amplitude (±200 V). The threshold energy of a given dissociation was determined using the curve-fitting and modeling program, CRUNCH, developed by Armentrout and co-workers.[28] All dissociations considered in this study were of the type $[M-L]^+$, where M = Na, K, or Ag and L = H_2O, H_2CO_3, glycine (G), proline (P), triglycine, and trialanine. Thus, the threshold energies measured are those of the bond dissociation energies of the metal−ion complexes. A more detailed discussion of the data treatment and additional details of the hardware are available in the Supporting Information.

RESULTS AND DISCUSSION

As stated in the introductory material, attention and care regarding a number of details[10,14,16] are required to ensure acquisition of high-quality data. The most important of these are the kinetic energy of the precursor ions, the intensity-to-cross-section conversion, the stability conditions of the ring ion guide, and the internal energy of the precursor ions. We shall delineate and discuss these subjects as they pertain to the ring ion guide before proceeding to the threshold-energy data.

Kinetic Energy of the Precursor Ions. In our tandem mass spectrometer, sampled ions suffer many collisions in q0, which has a nominal pressure of 8.5 mTorr. As a result, the q0 region acts as a source of thermalized ions for downstream events, and the potential experienced by the ions in q0 is, therefore, the reference point (sometimes referred to as the "zero point") for calculating the potential difference that accelerates the ions into the ring ion guide. However, the difference between the q0 dc offset (q0) and the ring ion guide dc offset (RO2) as set by the mass spectrometer software yields a nominal laboratory kinetic energy that is *not* adequate for use in TCID calculations, as the potential difference experienced by the ions inside the ion optics is modulated by local potential disturbances.[17,19] These include contact potentials and build up of surface charges that can increase significantly during experiments, necessitating regular determinations of the actual potential and the distribution of the kinetic energy during intervals between experiments. These determinations were made using a time-of-flight method, the details of which are available in the Supporting Information. Use of the retarding-field method for characterization of the precursor ion energy in our setup was found to be inadequate for the modified API 365 ion optics, see the Supporting Information for details.

Minimizing the quadrupole dc component minimizes rf heating, which modifies the kinetic energy distribution.[19] To reduce rf heating in TCID and kinetic energy distribution measurements, the resolution for Q1 and Q3 was optimized for each targeted ion to attain proper mass separation while keeping resolution relatively low; typically this resulted in a condition that was slightly lower than unit mass resolution. These conditions also minimized unwanted mass discrimination effects.[14] Routinely, a deviation between −0.36 and −0.90 eV (laboratory frame) from the absolute zero of the energy scale was measured together with a kinetic energy distribution between 0.59 and 0.96 eV (E_{lab}, fwhm), which is comparable to that in GIBMS (0.25−0.50 eV; note, however, that recently published numbers from a combination of ion funnel, hexapole ion guide, and GIBMS are lower at 0.09−0.20 eV).[29] The fwhm of a one-dimensional Boltzmann velocity distribution at 300 K for $[Na(H_2O)]^+$ is 0.08 eV and for $[Na(AAA)]^+$ 0.10 eV; the measured width is 0.59 eV for $[Na(H_2O)]^+$ and 0.69 eV for $[Na(AAA)]^+$.[10,29,30] The wider experimental distribution is probably a perturbation as a result of rf heating during passage of the ions through Q1. Radio frequency heating could be counteracted by the introduction of collisional cooling *after* mass selection, but would require major modifications to the ion optics. The width of the kinetic energy distribution, as determined by the TOF method, only reflects the axial component of the kinetic energy of the precursor ions. Although the transverse component of the kinetic energy remains to be determined, the use of tube lenses limits beam divergence and fringe fields and facilitates the formation of a well-defined ion energy distribution.[27,31]

Intensity-to-Cross Sections Conversions. The dissociation cross sections of the product ions were determined as a function of the center-of-mass energies at three collision gas pressures: 0.05, 0.10, and 0.15 mTorr above the background pressure of 5×10^{-6} Torr. The API 365 employs a channel electron multiplier for ion detection; a built-in discriminator module filters out detector background noise. In our experiments, argon was used as the collision gas; xenon would have been a suitable complementary collision gas for higher bond dissociation energies (see ref 32) but was not tested. To eliminate the effects

(27) Fite, W. L. *Rev. Sci. Instrum.* **1976**, *47*, 326–330.
(28) Ervin, K. M.; Armentrout, P. B. *CRUNCH*, version 5.0; 2005.
(29) Moision, R. M.; Armentrout, P. B. *J. Am. Soc. Mass Spectrom.* **2007**, *18*, 1124–1134.
(30) Chantry, P. J. *J. Chem. Phys.* **1971**, *55*, 2746–2759.
(31) Smolanoff, J.; Lapicki, A.; Anderson, S. L. *Rev. Sci. Instrum.* **1995**, *66*, 3706–3708.
(32) Aristov, N.; Armentrout, P. B. *J. Phys. Chem.* **1986**, *90*, 5135–5140.

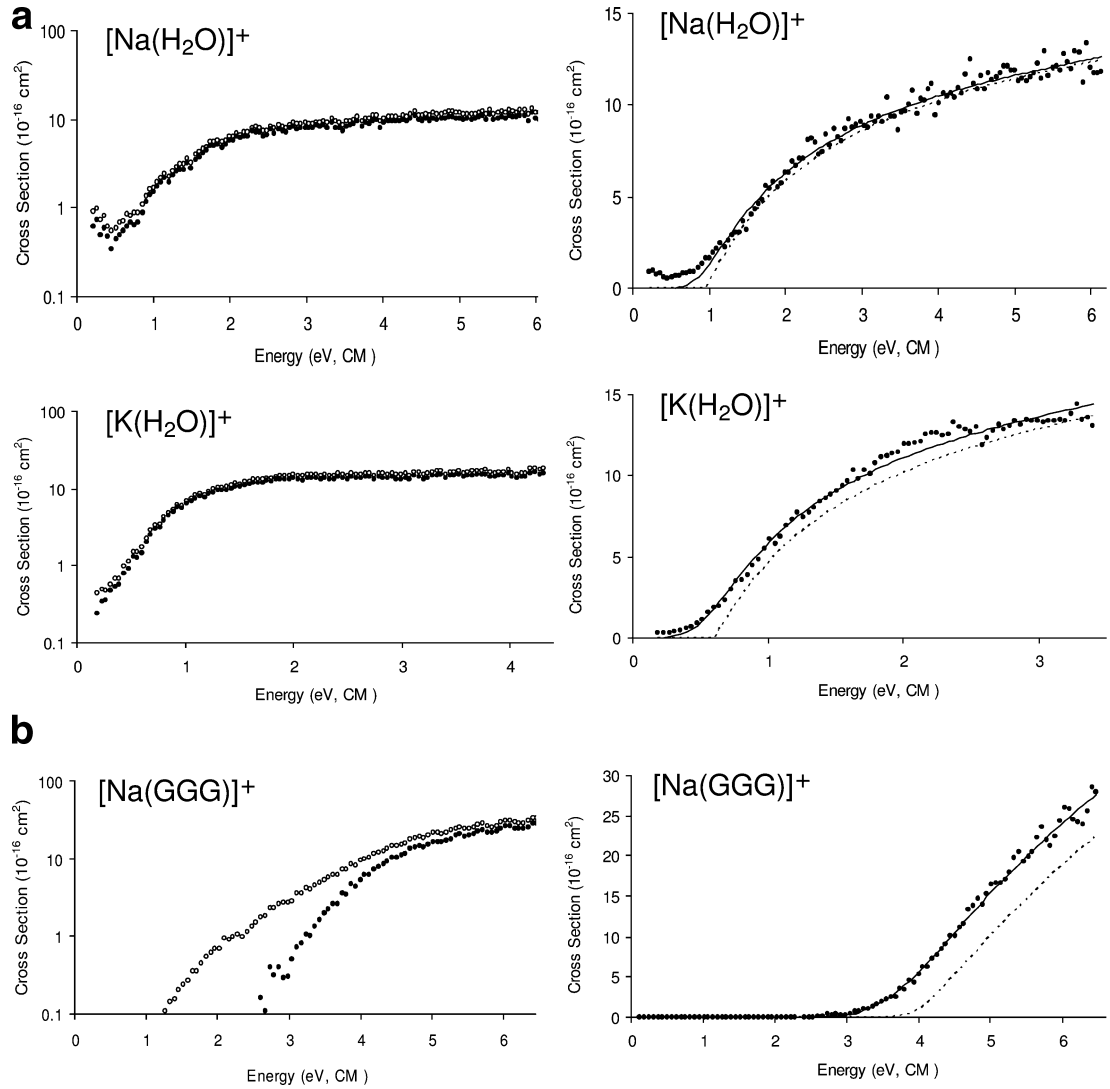

Figure 2. (a) Single TCID semilog (left panels) and linear (right panels) plots recorded with (●) and without (○) background subtraction for $[Na(H_2O)]^+$ (top panels) and $[K(H_2O)]^+$ (bottom panels). The E_0(PSL) for $[Na(H_2O)]^+ = 0.99$ with background correction and 0.96 eV without background correction. The E_0(PSL) for $[K(H_2O)]^+ = 0.96$ eV with background correction and 0.70 eV without background correction. PSL: phase space limit; E_0 (PSL) are bond energies for which the kinetic shifts have been corrected. Although of no effect on the TCID determination, deviation of the cross sections at low energies from the expected trend was observed for the sodium complex possibly as a result of sodium ion trapping inside the ring ion guide. (b) The effect of background subtraction for a large ion, $[Na(GGG)]^+$. Single TCID linear plots (left panel) and semilog plots (right panel) recorded with (●) and without (○) background subtraction. For curve-fitting the full range was used, yielding an E_0(PSL) = 2.46 eV with and 1.53 eV without background subtraction, thereby illustrating the necessity of proper background correction for larger ions.

of multiple collisions, E_0 values were obtained from threshold curves constructed from $\sigma(E)$ at zero pressure. The latter data were determined by linear extrapolation of the $\sigma(E)$ measured at the three pressures to zero pressure. Conversion of the measured intensities to cross sections requires the pressure as well as the effective length of the collision cell. Different ways of estimating the effective length of a collision cell have been reported,[33] but only the Howard−Mathur model[34,35] is supported by experimental results.[36] Under effusive flow conditions, the Howard−Mathur model predicts a correction factor close to unity for the effective length in a collision cell whose length is much larger than its orifice diameter.[33,36] In our calculations, the effective length was taken as being the cell's geometric length. An experimental determination of the effective length is planned in a future study.

Background ions can result from dissociations occurring outside the collision cell, e.g., those as a consequence of precursor ion acceleration between Q1 and the collision cell, and (to a lesser extent) between the collision cell and Q3. Following the basic protocol outlined in ref 10, to test the effect of background ion generation, collision gas was diverted from the collision cell to the vacuum chamber at set pressures of 0.05, 0.10, and 0.15 mTorr. Collisional cross sections were measured with and without diverting the gas, and the difference for each data point was used to construct the background-subtracted TCID curve. Although no difference in pressure was recorded by the Bayard−Alpert gauge with and without gas diversion, both cross sections and derived dissociation energies clearly show the effect of background ion generation, see Figure 2 for typical results. The dissociation energies displayed a clear trend for E_0 measured with and

Table 2. Equations Used for Deriving Ring Ion Guide Stability Conditions[a]

$$V_{\text{eff}}(\mathbf{r},\mathbf{z}) = \frac{(qV_0)^2 A}{4m\Omega^2} \quad (4)$$

$$\eta(\mathbf{r},\mathbf{z}) = \frac{qV_0\sqrt{2}B}{m\Omega^2} \quad (5)$$

$$A = \frac{I_0^{\,2}(\mathbf{r})\sin^2(\mathbf{z}) + I_1^{\,2}(\mathbf{r})\cos^2(\mathbf{z})}{z_0^{\,2}I_0^{\,2}(\mathbf{r}_0)} \quad (6)$$

$$B = \sqrt{\frac{(I_0^{\,2}(\mathbf{r}) - I_1^{\,2}(\mathbf{r}))^2\sin^2(2\mathbf{z})}{z_0^{\,4}I_0^{\,2}(\mathbf{r}_0)(I_0^{\,2}(\mathbf{r})\sin^2(\mathbf{z}) + I_1^{\,2}(\mathbf{r})\cos^2(\mathbf{z}))}} \quad (7)$$

[a] $\mathbf{r}$, $\mathbf{r_0}$, $\mathbf{z}$, reduced variables $\mathbf{r} = r/z_0$, $\mathbf{r_0} = r_0/z_0$, $\mathbf{z} = z/z_0$ with radial coordinate $r(m)$, axial coordinate $z(m)$, $z_0 = d/\pi$ with $d(m)$ = distance between the middle of the two rings; r_0, (m) aperture radius; V_0, (V) half the applied peak-to-peak voltage with angular frequency $\Omega = 2\pi f$ (s^{-1}); q, m, charge (C) and mass of the ion (kg); I_0, I_1, zero and first-order modified Bessel functions; $V_{\text{eff}}(\mathbf{r},\mathbf{z})$, (eV).

without background correction: the larger the bond energy of the complex, the larger the background correction. It is to be noted that the background pressure (5×10^{-6} Torr) of the API 365 is higher than that of a GIBMS (1×10^{-7} Torr);[10] thus, the potential for generating background ions is higher in the former than in the latter instrument. In fact for $[Na(AAA)]^+$, whose M^+-L bond dissociation energy is among the largest, background correction was mandatory for proper curve-fitting by CRUNCH. In conclusion, background corrections were proven to be necessary and therefore, following Ervin and Armentrout,[10] included in all our measurements.

Stability Conditions of the Ring Ion Guide. An analytical approximation for the effective field $V_{\text{eff}}(\mathbf{r},\mathbf{z})$ created by a stack of rings has been derived by Gerlich,[19] see Table 2, eq 4. A steeper $V_{\text{eff}}(\mathbf{r},\mathbf{z})$ is obtained by increasing $\mathbf{r} = r_0/z_0 = r_0/(d/\pi)$ through a decrease in the distance d between the rings. To derive this equation, use was made of the adiabatic approximation. The adiabatic approximation of ion motion in an effective field generated by a fast oscillatory (rf) field consists of separating the ion motion into a slow (secular, macro or thermal) motion of large amplitude, and a fast (rf or micro) motion of small amplitude. This approximation is only valid under certain conditions as expressed by the adiabaticity parameter $\eta(\mathbf{r},\mathbf{z})$ (Table 2, eq 5).[37] For $\eta < 0.3$, the ion trajectory is stable over the length of the ring ion guide and the effective potential is described by eq 4 in Table 2; the change of the field over the oscillation is much smaller than the field itself.[19] For $\eta > 0.3$, the separation of ion motion into a secular and rf contribution is no longer valid, the ion trajectory becomes unstable and ions absorb energy supplied by the rf field—a condition to be avoided in TCID measurements. The operation of the ring ion guide is limited at the low-mass range by the value of the adiabaticity parameter and at the high-mass range by the steepness of the effective potential that determines the containment of ions with a *transverse* kinetic energy E_m. Using the conditions

$$\eta(m_{\text{min}}) \leq 0.3 \quad (8)$$

$$V_{\text{eff}}(m_{\text{max}}) \geq E_m \quad (9)$$

the supply voltage and frequency of the rf voltage can be derived, see eqs 10 and 11, with f in megahertz, E_m in electronvolts, V_0 in volts, m in unified atomic mass units, charge unit e_0, and $r_0 = 0.25$ cm (for the definitions of A and B, see Table 2, eqs 6 and 7, respectively).

$$f \geq f_{\text{min}} = 1.5\left(\frac{B}{\sqrt{A}}\right)\frac{\sqrt{E_m}\sqrt{m_{\text{max}}}}{m_{\text{min}}} \approx 8.09\frac{\sqrt{E_m}\sqrt{m_{\text{max}}}}{m_{\text{min}}} \quad (10)$$

$$V_0 = 18.9\frac{E_m m_{\text{max}} B}{m_{\text{min}} A} \approx 14.7\frac{E_m m_{\text{max}}}{m_{\text{min}}} \quad (11)$$

For calculation of the optimal operating frequency and voltage of the ring ion guide, conservative values for r ($0.8r_0$) and η (<0.3) are used. With the maximum values for ratios $(B/\sqrt{A})$ and (B/A), practical approximations for V_0 and f are obtained. With the use of these equations, operating conditions (V_0, f) can be derived. Calculations indicate that, under our experimental conditions, the ring ion guide was operating within the derived optimum limits, see Supporting Information for further details. Inspection of eq 4 in Table 2 further indicates that the effective potential of a ring ion guide has a weak undulation in the axial direction. The valleys could trap product ions, an effect that can be minimized by increasing the frequency and lowering the V_0. For ions of 23 and 39 Da at 5.4 MHz and $V_0 = 10$ V, a trapping potential of 7×10^{-6} and 4×10^{-6} V are obtained (using $r = 0$, $z = d/2$) along the central axis of the ring ion guide, and 0.05 and 0.03 V at $r = 0.8r_0$. For product ions of larger mass, trapping is less likely based on these operating conditions; however, for Na^+, inadvertent trapping occasionally occurs, see the section Bond Dissociation Energy Determinations. It should be pointed out that the derived equations are *approximations*; although a wide variation of the obtained values before the onset of instability is allowed, experimental support for the assumed stability needs to be established (vide infra).

Internal Energy of the Precursor Ions. As indicated in the introductory material, precursor ions subjected to threshold induced dissociation will need to have a well-defined internal energy following a Maxwell−Boltzmann distribution. Some uncertainty surrounds the amount of energy acquired by gas-phase ions created by electrospray ionization.[38] In addition, the combina-

(33) Blaauw, H. J.; Wagenaar, R. W.; Barends, D. H.; de Heer, F. J. *J. Phys. B: Atom. Mol. Phys.* **1980**, *13*, 359–376.
(34) Mathur, B. P.; Field, J. E.; Colgate, S. O. *Phys. Rev. A.* **1975**, *11*, 830–833.
(35) Howard, W. M. *Phys. Fluids* **1961**, *4*, 521–524.
(36) Wagenaar, R. W.; de Heer, F. J. *J. Phys. B: At. Mol. Phys.* **1985**, *18*, 2021–2038.

Table 3. Comparisons of Bond Energies Obtained Using TCID on the Modified API 365, Literature Values, and High-Level First-Principle Calculations

	complex	E_0 (PSL) (eV)[a]	reference and method used[b]
1	$[K(H_2O)]^+$	**0.73 ± 0.09**	present study, continuous beam
		0.78[c]	HPMS[d]
		0.74 ± 0.10[c]	HPMS[e]
2	$[K(H_2CO_3)]^+$	**1.02 ± 0.17**	present study, continuous beam
		0.97	present study, CCSD/6-311++G(d,p)
3	$[Na(H_2O)]^+$	**1.03 ± 0.12**	present study, continuous beam
		0.98 ± 0.08	GIBMS, DC/FT[f]
		1.05 ± 0.10[c]	HPMS[e]
		1.04[c]	HPMS[d]
4	$[Na(H_2CO_3)]^+$	**1.24 ± 0.15**	present study, continuous beam
		1.22	present study, CCSD/6-311++G(d,p)
5	$[Ag(H_2O)]^+$	**1.32 ± 0.09**	present study, continuous beam
		1.33 ± 0.07	present study, pulsed beam with trapping in q0
		1.36 ± 0.08	GIBMS, DC/FT[g]
		1.44 ± 0.10[c]	HPMS[h]
6	$[Na(G)]^+$	**1.73 ± 0.12**	present study, continuous beam
		1.70 ± 0.05	GIBMS, DC/FT[i]
		1.57 ± 0.10	TCID, ESI[j]
		1.67 ± 0.12[c]	ICR EQ[k]
		1.67 ± 0.08	KM[l]
		1.65 ± 0.21[c]	KM[m]
7	$[Na(Pro)]^+$	**1.97 ± 0.13**	present study, continuous beam
		1.94 ± 0.08	GIBMS, ESI[n]
		1.93 ± 0.06	GIBMS, DC/FT[o]
		1.81 ± 0.12[c]	ICR EQ[p]
		2.03 ± 0.08	KM[l]
8	$[Na(GGG)]^+$	**2.42 ± 0.17**	present study, continuous beam
		2.53 ± 0.15	present study, pulsed beam with trapping in q0
		2.49 ± 0.18	GIBMS, ESI[q]
		2.45 ± 0.09	KM[r]
9	$[Na(AAA)]^+$	**2.49 ± 0.31**	present study, continuous beam
		2.51 ± 0.09	KM[r]

[a] Standard error of the mean at 90% confidence interval, for data obtained with ring ion guide in bold, experiments performed in quadruplicate or $n = 4$. PSL, phase space limit; E_0 (PSL) are bond energies for which the kinetic shifts have been corrected. [b] GIBMS, guided ion beam mass spectrometry; ESI, electrospray ionization source; DC/FT, discharge/flow tube source; TCID, threshold collision-induced dissociation on a modified triple quadrupole mass spectrometer; HPMS, high-pressure mass spectrometry; KM, kinetic method; ICR EQ, ion cyclotron resonance equilibrium. [c] At 298 K. [d] Kebarle et al., *J. Phys. Chem.* **1970**, *74*, 1466. [e] Burdett and Hayhurst *J. Chem. Soc. Far. Trans. I* **1982**, *78*, 2997. [f] Dalleska et al., *J. Phys. Chem.* **1994**, *98*, 4191. [g] Armentrout et al., *Int. J. Mass Spectrom.* **2003**, *228*, 221. [h] Holland and Castleman, *J. Chem. Phys.* **1982**, *76*, 4195. [i] Armentrout et al., *J. Chem. Phys.* **2002**, *106*, 10350. [j] Kebarle et al., *J. Phys. Chem.* **1996**, *100*, 14218. [k] Dunbar et al., *Int. J. Mass Spectrom.* **2003**, *228*, 825. [l] Wesdemiotis et al., *Int. J. Mass Spectrom.* **2003**, *227*, 509. [m] Andersen et al., *Org. Mass Spectrom.* **1993**, *28*, 1448. [n] Armentrout et al., *J. Am. Soc. Mass Spectrom.* **2007**, *18*, 1124. [o] Armentrout et al., *J. Am. Chem. Soc.* **2006**, *110*, 3933. [p] Dunbar et al., *Int. J. Mass Spectrom.* **2003**, *228*, 825. [q] Armentrout et al., *J. Chem. Phys. A* **2008**, *112*, 3587. [r] Wesdemiotis et al., *J. Am. Soc. Mass Spectrom.* **2007**, *18*, 541.

tion of supersonic expansion (resulting in cooling of the ions) and subsequent collisional heating adds further uncertainty with regard to the actual internal energy of the gas phase ions. A sufficiently large number of collisions with gas molecules will result in thermalization of the ions to a well-defined internal energy, but a cursory investigation of the literature indicates a range of $10-10^5$ collisions are required for thermalization.[29,39−42]

Triple-quadrupole mass spectrometers in general use collisional focusing in order to increase ion throughput in the front end (q0) and collision cell (q2).[43] The increased pressure slows down the ions and, in addition, narrows the internal energy distribution.[43] Two different approaches were taken to determine if sufficient thermalization takes place in q0 for the ions to be used in TCID experiments. One approach consisted of determining the average number of collisions at the q0 operating pressure (8.5 mTorr nitrogen) by measuring the average time an ion pulse requires to move through the q0 region. By pulsing either the focusing ring electrode (open 1 ms at +85 V, close 200 ms at −85 V) or the IQ1 lens (open 5 μs at −3 V, close 2 ms at +3 V, see Figure 1), arrival time distributions were recorded for $[Ag(CH_3OH)]^+$ (m/z 139) and $[hemin]^+$ (m/z 616) using a multichannel scaler from which the mean values of the arrival times of the ions were calculated by integration over the arriving ion profiles.[44] Correction for the time of travel outside q0 yields average residence times in q0 of 25 ± 1 and 28 ± 1 ms for $[Ag(CH_3OH)]^+$ and $[hemin]^+$, respectively. For a q0 length of 18 cm, average velocities of 7.1 and 6.4 m/s were calculated for $[Ag(CH_3OH)]^+$ and $[hemin]^+$, considerably below their thermal velocities of 233 and 111 m/s, respectively,

(37) Savić, I. Ph.D. Dissertation, Technische Universitat Chemnitz, Chemnitz, Germany, 2004.
(38) Gabelica, V.; De Pauw, E.; Karas, M. *Int. J. Mass Spectrom.* **2004**, *231*, 189–195.
(39) Baranov, V. I.; Tanner, S. D. *J. Anal. At. Spectrom.* **1999**, *14*, 1133–1142.
(40) Koslovsky, V.; Fuhrer, K.; Tolmachev, A.; Dodonov, A.; Raznikov, V.; Wollnik, H. *Int. J. Mass Spectrom.* **1998**, *181*, 27–30.
(41) Tolmachev, A. V.; Udseth, H. R.; Smith, R. D. *Int. J. Mass Spectrom.* **2003**, *222*, 155–174.
(42) Schultz, R. H.; Armentrout, P. B. *Int. J. Mass Spectrom. Ion Processes* **1991**, *107*, 29–48.
(43) Douglas, D. J.; French, J. B. *J. Am. Soc. Mass Spectrom.* **1992**, *3*, 398–408.
(44) Krutchinsky, A. N.; Chernushevich, I. V.; Spicer, V. L.; Ens, W.; Standing, K. G. *J. Am. Soc. Mass Spectrom.* **1998**, *9*, 569–579.

as a result of the gas pressure in q0.[44] Comparable values for the mean ion velocities of ions differing considerably in mass are interpreted to be due to diffusion through q0, which should allow ample time for thermalization. The average number of collisions at a pressure of 8.5 mTorr nitrogen can be calculated using a trajectory collision model,[45] which yields average numbers of collisions for $[Ag(CH_3OH)]^+$, 4 498 ± 213, and for $[hemin]^+$, 4 745 ± 167 collisions. These numbers approach the upper limit of the number of collisions (10^5) considered to be sufficient for thermalization.[29,46] To further substantiate the thermalization of electrospray ions in q0, a *pulsed* TCID experiment was performed using $[Ag(H_2O)]^+$ and $[Na(GGG)]^+$. According to the trajectory collision model,[45] storing $[Ag(H_2O)]^+$ and $[Na(GGG)]^+$ ions for 600 ms at 8.5 mTorr would result in 1.1×10^5 and 1.0×10^5 collisions, respectively. These are numbers that have been shown to be sufficiently large for thermalization in GIBMS.[29] After a 100 ms ion pulse using the ring electrode (open 100 ms at +85 V, closed 600 ms at −85 V), ions were stored in q0 for 600 ms by keeping IQ1 at +3 V. At the ion release pulse (open IQ1 30 ms at −3 V), ions were accelerated into the collision cell. By repeated cycling through the fill time (100 ms), cool time (600 ms), and ion release (30 ms), a TCID curve was created by varying the offsets of RO2, RO3, and IQ3. The TCID results obtained in the pulsed mode, i.e., using trapping in q0, and in the continuous mode are within the error margin between each other and with those obtained on GIBMS (Table 3: items 5 and 8). This substantiates that ions $[Ag(H_2O)]^+$ and $[Na(GGG)]^+$ were thermalized in both the continuous and pulsed modes of operation.

Bond Dissociation Energy Determinations. Under the conditions described, TCID data were obtained for a set of compounds of known bond dissociation energies (see Table 3, items 1, 3, and 5−8) for validation purposes and for extension of the data (see Supporting Information for details). As a group, accurate data were obtained using the described operating conditions over a bond dissociation energy range of 0.73−2.42 eV (17−56 kcal/mol), and all within the error margin of the corresponding literature values. A closer inspection of individual TCID curves revealed for $[Na(H_2O)]^+$ (see Figure 2a, top panel) larger than expected cross sections between 0 and 0.5 eV (E_{cm}). This phenomenon was not readily reproducible but builds up and persists through a series of experiments independent of ion optics settings. Similar observations have been made using an octopole ion guide by Ervin et al.[47] who, after a series of diagnostic experiments, concluded these observations were due to inadvertent trapping of ions. Investigation of the trapping potential as generated by the rf resonant circuit (vide supra and Figure 1) indicates a trapping potential of 0.05 and 0.03 V (at $r = 0.8r_0$) for, respectively, the sodium and potassium ion, i.e., around the thermal energy of the ions (0.039 eV). Considering the limitations of the equations in Table 2, the absence of this effect in the TCID curves of $[K(H_2O)]^+$ may be fortuitous.

In addition, a series of compounds for which no TCID bond dissociation energies are available were used on the ring ion guide setup and the results compared with high-level theoretical calculations, the details of which are available in the Supporting Information. The sodium and potassium adducts of carbonic acid have attracted our attention because of the ease with which these ions are formed under electrospray conditions. Bond dissociation measurements (Table 3, items 2 and 4) gave energies in excellent agreement with calculated bond energies at the CCSD/6-311++G(d,p) level of theory. For $[Na(AAA)]^+$, a bond dissociation energy of 2.49 eV was measured using the TCID method, which is comparable to the value of 2.51 eV obtained by Wesdemiotis et al. using the kinetic method (see Table 3, item 9). However, the error margin for this series of measurements (±0.31 eV) is substantially higher than those for other series (see Table 3), as a result of the borderline acceptable operating conditions for this ion, which required an ion kinetic energy of 36 eV (E_{lab}) for the threshold onset combined with a large kinetic shift and corresponding uncertainty of 2.37 ± 0.19 eV.

It is readily apparent that a limitation of the present setup is due to the use of a resonant rf driver. Use of an rf driver at higher frequencies that can be triggered should allow the determination of the useful range of the ring ion guide over a series of rf amplitudes and would allow testing of the effect of ion trapping in the ring ion guide. Other areas that could offer further improvement are related to increasing the sampling efficiency, which will increase the precursor ion influx and signal-to-noise ratios of the ions, and to minimizing the background correction by decreasing the pressure in the vacuum chamber.

CONCLUSIONS

On the basis of the aforementioned measurements, an energy range of 16−57 kcal/mol appears accessible using our modified instrumentation. The bond dissociation energies measured with this ring ion guide setup are in good agreement with those obtained with GIBMS. The modifications and adaptations necessary are relatively minor, thus making this approach a valuable option for users of triple-quadrupole mass spectrometry to implement TCID measurements.

ACKNOWLEDGMENT

We thank Peter B. Armentrout for making the CRUNCH program available to us, as well as for his valuable insights regarding TCID. We are in debt to a number of MDS Analytical Technologies scientists, including John Vandermey for help with the electronics, Pablo Dominguez for the design and construction of the ring ion guide, and Bruce Thomson and Vladimir Baranov for very informative discussions. This work was supported by the Natural Sciences and Engineering Research Council (NSERC) of Canada and MDS Analytical Technologies. V.R. thanks the Ontario Graduate Scholarship in Science and Technology for financial support.

SUPPORTING INFORMATION AVAILABLE

Details of hardware modifications, determination of the reference (zero) point of the energy scale, optimal conditions of the ring ion guide, experimental uncertainties, details of the calculations, TCID figures and data, and Cartesian coordinates, rotational constants, and vibrational frequencies. This material is available free of charge via the Internet at http://pubs.acs.org.

Received for review May 5, 2009. Accepted July 7, 2009.

AC9009758

(45) Su, T.; Chesnavich, W. J. *J. Chem. Phys.* **1982**, *76*, 5183–5185.
(46) Muntean, F.; Armentrout, P. B. *J. Chem. Phys.* **2001**, *115*, 1213–1228.
(47) DeTuri, V. F.; Hintz, P. A.; Ervin, K. M. *J. Phys. Chem. A* **1997**, *101*5969–5986.